SAND96-3027C
CONF-970616--5

An Engineering Model to Simulate the Thermal Response of Electronic Devices During Pulsed Nd:YAG Laser Welding

S.E. Gianoulakis, T. E. Voth, P.W. Fuerschbach

Sandia National Laboratories

Engineering Sciences Center

MS 0835

P.O. Box 5800

Albuquerque, NM 87185

and

J. H. Prinzbach

Technology Department

Wilson Greatbatch Ltd.

Clarence, NY

DISCLAIMER

ABSTRACT

A model is developed to predict the thermal response of "real" electronic devices during pulsed Nd:YAG laser welding. Modeling laser-part interaction requires incorporation of weld pool hydrodynamics, and laser-metal vapor and laser-surface interactions. Although important information can be obtained from these models, they are not appropriate for use in design of actual components due to computational limitations. In lieu of solving for these detailed physics, a simple model is constructed. In this model, laser-part interactions are accounted for through an empirically determined energy transfer efficiency which is developed through the use of modeling and experiments. This engineering model is appropriate since part thermal response near the weld pool and weld pool shape is not of interest here. Reasonable agreement between predictions and experimental measurements for welding of real components are indicated.

NOMENCLATURE

c	specific heat
d	beam diameter
E	total energy per laser pulse
ETE	energy transfer efficiency
f	laser focal length
f	beam pulse rate
h	convection coefficient
k	thermal conductivity
L	weld pool width
P	beam power
Pe	Peclet number, $d \cdot V/\alpha$
q"	laser induced surface heat flux
s	location of beam center along beam path
t	time
t_{dp}	pulse duration
T	temperature
T_o	maximum weld pool surface temperature
U_σ	weld pool velocity scale
V	laser travel speed
x	x-coordinate
y	y-coordinate
z	z-coordinate

Greek

α	thermal diffusivity, $k/\rho \bullet c$
ΔT	weld pool surface temperature difference, $(T_o - T_l)$
δ	weld pool length scale
ε	emissivity
λ	latent heat of fusion
μ	absolute viscosity
ρ	density
θ	dimensionless temperature, $(T - T_i)/(T_l - T_i)$
σ_T	rate of change of surface tension with temperature

Subscripts

a	absorbed
avg	time averaged quantity
e	end location
d	development experiment thermocouple location
i	initial
j	coordinate index
m	modified thermophysical property
l	liquidus
o	initial location
p	process experiment thermocouple location
peak	peak

s	solidus
x	x-direction
y	y-direction
z	z-direction

INTRODUCTION

Hermetic containers are employed to package many types of electronic devices and components used in modern technology. These containers typically serve as an environmental barrier to extend life and improve reliability of the components being packaged (Seraphim et al., 1989). One approach to sealing the hermetic packages is a closure weld. When closure welding small electronic packages containing glass-to-metal seals (see Fig. 2), the thermal stresses that develop in the glass are of concern (Gianoulakis et al., 1995). If these stresses exceed allowable tensile levels, the glass may crack resulting in a loss of hermeticity. Closure welding normally occurs near the end of the assembly process and failure of a glass seal typically dictates that the entire component be scrapped or reworked, often at substantial cost.

A thorough understanding of how welding processes affect the stresses in glass-to-metal seals is desirable from a reliability standpoint and for the development of an optimum welding schedule. There are several approaches that can be taken to minimize the possibility of cracking the glass seals. These approaches include designing special weld joint geometries which act to minimize the required heat input, using high power density, low-total heat input welding processes such as laser and electron beam, keeping the seals as far as possible from the weld, and process optimization (Knorovsky and Burchett, 1989). A "trial and error" approach is often used in an attempt to optimize the weld design process. This method is quite slow and expensive. With electronic components becoming smaller, and time to market and product cost issues becoming more important, a more fundamental understanding, and the ability to model the coupled thermal-mechanical interactions during welding are becoming more necessary than ever.

To accurately model the response of seals during laser welding, the overall thermal response of the package must be predicted. Asymmetric thermal loadings on the glass seal will

occur as the weld travels along the perimeter of the package. Proper modeling of the weld region, which is the source of thermal energy in the component, ideally should include the solution of the conjugate heat transfer problem including the effects of laser-vapor plume interaction, surface depression, surface tension driven flow, and phase change. To simulate the closure welding of a "real" component, inclusion of all these phenomena would result in an intractable problem using current computing tools. This paper describes the development and experimental validation of an engineering model which can predict the thermal response of temperature sensitive parts during pulsed Nd:YAG laser welding processes. The model is designed to account for the relevant phenomena that occur within a weld pool, and simulate the thermal response with conduction heat transfer.

EXPERIMENTAL PROGRAM

The experimental investigation is broken into i) model development experiments and ii) actual process experiments. All experiments incorporate a part subject to pulsed Nd:YAG laser welding. The model development experiments (Fig. 1) are designed to provide the thermal response history of a simple part. The thermal histories obtained from the development experiments are used to estimate energy transfer efficiencies for the specific process studied (e.g. 304 stainless steel and pulsed Nd:YAG laser). The process experiments (Fig. 2) are designed to simulate an actual welding process where an electronic component is welded to create a hermetic seal between the case and header. Process experiment measurements are compared to predictions to validate the model. The details of the experiments are discussed below.

Model Development Experiments

The model development experiments (Fig. 1) are designed so that laser travel speed (V), time averaged beam power (P_{avg}), beam peak power (P_{peak}), pulse rate (f) and beam diameter (d)

are within expected ranges for representative welding process used for micro-electronic package manufacturing (Honegger, 1996). The ranges considered are V = 15.2 mm/s, P_{avg} = 150 W, P_{peak} = 550 - 2770 W, f = 35 - 208 pulse/s, and d = 0.61 mm (see Table 4 for details).

The apparatus consists of a pulsed Nd:YAG laser and a fixture designed to translate the part underneath the beam. The beam is focused on the flat 304 stainless steel plate (see Table 1 for properties) where appropriate dimensions are indicated in Fig. 1. The part is moved so that the beam is translated across it as illustrated in Fig. 1. The thermal response of the part is measured with six 254 μm chromel-alumel thermocouples attached to the bottom surface of the plate. Thermocouple data are collected at 3 millisecond intervals. A detailed description of the experimental apparatus is provided in (Fuerschbach and Hinkley 1997).

Process Experiments

The apparatus used in the process experiments is similar to that used in the development experiments with the exception that the stainless steel flat plate is replaced by the electronic component illustrated in Fig. 2. As illustrated in Fig. 2, the component consists of a 0.762 mm thick 304 stainless steel header which is to be welded to a case (of the same material) of 0.381 mm wall thickness (other dimensions are illustrated in Fig. 2). Inserted in the lid is a 304 stainless steel ferrule (1.65 and 4.19 mm inner and outer diameters respectively) through which passes a 0.50 mm diameter molybdenum pin. The pin is fixed in the ferrule with a low thermal expansion glass. Thermal properties for these materials are listed in Tables 1, 2, and 3.

The laser beam begins translating in a clockwise direction around the lid-case seam at a fixed velocity. When the beam reaches location s_o shown in Fig. 2, the beam is energized and continues to translate around the seam until it returns to its starting location. The beam then continues an additional 3.6 mm to create a slight seal overlap, ending at location s_e shown in Fig. 2. Process-

ing parameters of V = 15.2 mm/s, and P_{peak} = 1390 and 830 W (f = 83 and 138 pulse/s respectively) were considered as they are representative of actual processing conditions. As in the development experiments d = 0.61 mm and P_{avg} = 150 W are used.

The thermal response of the part is measured with four 254 μm chromel-alumel thermocouples. As shown in Fig. 2, two of the thermocouples are placed on the underside of the header, one is located on the outer surface of the case and one on the surface of the ferrule.

All experiments were repeated at least twice to assess the reproducibility of the measurements. Thermocouple uncertainties are estimated to be ± 3.0 K while thermocouple placement errors where found to be approximately ± 0.02 mm. Together, these uncertainties resulted in the experiments being repeatable to within $\Delta\theta = \pm 0.03$.

THE MODEL

Computational geometries for the development and process simulations are shown in Figs. 1 and 2. All thermal properties are assumed to be temperature dependent (see Tables 1, 2 and 3). The governing equations are solved using COYOTE, a finite element code developed to solve nonlinear diffusion problems (Gartling and Hogan, 1994).

Heat Diffusion Model:

The equation for thermal transport in the parts is:

$$\rho c_m \frac{\partial T}{\partial t} = \frac{\partial}{\partial x}\left(k_{m,x}\frac{\partial T}{\partial x}\right) + \frac{\partial}{\partial y}\left(k_{m,y}\frac{\partial T}{\partial y}\right) + \frac{\partial}{\partial z}\left(k_{m,z}\frac{\partial T}{\partial z}\right) \qquad (1)$$

where variable properties have been assumed to account for temperature dependence. In Eqn. (1) specific heat, c, has been modified to account for latent heat effects during solid-liquid phase

change,

$$c_m = c + \frac{T_l - T_s}{\lambda} \qquad T_s \le T \le T_l$$
$$c_m = c \qquad otherwise \tag{2}$$

where T_s and T_l are the solidus and liquidus temperatures and λ is the latent heat of fusion (for 304 stainless steel T_s = 1670 K, T_l = 1730 K, λ = 2.65 x 105; Choi et al., 1987). This method of modeling phase change requires care in the choice of time step such that the phase change effect is not missed (Zienkiewicz and Taylor, 1991). To avoid this problem a maximum temperature step of (T_l - T_s)/5 is imposed and time steps are adjusted to meet this criterion. A typical time step using this criterion is 1.0 x 10^{-3} s.

The boundary conditions in the model include natural convection and radiation to the surroundings. Numerical experiments showed that boundary conditions had only minimal influence on the thermal response of the parts (less than 2% change in weld pool surface θ for $5 < h < 50$ W/m^2K) during the early phase of the process ($t < 10$ s). For this reason, and because only the early thermal response of the parts is of interest here, detailed convection and radiation models are not used. Rather, simple convection correlations for vertical surfaces (Incropera and DeWitt, 1990) and gray body radiation relations (Siegel and Howell, 1992) were used (ε = 0.33, 0.80 and 0.80 for stainless steel, molybdenum and glass respectively; Incropera and DeWitt, 1990).

Laser Beam Model

The laser beam is modeled as a uniform heat flux boundary condition (top-hat distribution) imposed over a circular region. The assumption of a top-hat laser energy distribution is reasonable since the beam considered here is delivered to the workpiece through a fiber-optic system

which results in an approximately constant radial laser intensity,

$$q'' = \frac{ETE \bullet P_{avg}}{(\pi d^2/4)} \tag{3}$$

where ETE is the energy transfer efficiency (defined later). Assuming square-wave laser pulses, conservation of pulse energy results in $P_{avg} = P_{peak} \bullet t_{pd} \bullet f$ where t_{pd} is the pulse duration of the square-wave pulse. In this work, $t_{pd} = 1.3 \times 10^{-3}$ s.

To model the translation of the laser beam, the heat flux area is moved over the surface of the part so that at any time the center of the area is located at,

$$s(t) = s_o + \int_0^t V(t)dt \tag{4}$$

where s_o is the initial location of the beam center.

Weld Pool Model

Because the thermal response of the part in and very near the weld pool is not of interest here, detailed modeling of weld pool physics is not necessary. In fact, detailed modeling of the weld pool physics requires incorporation of complex physics which include buoyancy and surface tension driven convection, solid-liquid and liquid-vapor phase change, laser-vapor plume interactions and pool surface deflections (Root, 1980; Oreper and Szekely, 1984; Chen, 1987; Russo et al., 1990; Kanouff and Greif, 1992). Because of the complex nature of these phenomena, significant computational resources are necessary to model even simple weld pool geometries where stationary, continuous laser beams are simulated (Russo et al., 1990). Because this model is designed to simulate the far-field thermal response of "real" components, a simple model of the weld pool physics is considered appropriate (far-field implies at least one laser beam diameter from the weld).

In order to account for convective transport in the weld pool, thermal conductivity of the melt is enhanced relative to the thermophysical value. The enhanced (or modified) thermal conductivity,

$$k_{m,j} = k + c(\mu\rho\sigma_T\Delta TL)^{1/3} \quad j = x, y$$
$$k_{m,j} = k \qquad j = z \tag{5}$$

suggested by Kanouff (1994), relates $k_{m,j}$ to the thermophysical properties of the molten metal, dimensions of the weld pool, L, and temperature difference across the weld pool's surface, ΔT (note that Eqn. (5) assumes that the weld pool surface is in the x-y plane). Equation (5) is based on velocity and length scales,

$$U_\sigma = \left(\frac{\sigma_T{}^2\Delta T^2}{\rho\mu L}\right)^{1/3} \tag{6}$$

$$\delta = \left(\frac{\mu^2 L^2}{\rho\sigma_T\Delta T}\right)^{1/3} \tag{7}$$

where σ_T, ρ and μ are the rate of change of surface tension with temperature, density and viscosity ($\sigma_T = 4.0 \times 10^{-4}$ N/m•K and $\mu = 6.5$ x 10-3 kg/m•s; Russo et al., 1990). These scales were developed originally for thermocapillary driven flow with conditions similar to those in weld pools (Ostrach, 1982; Kanouff, 1994). Using Eqns. (6) and (7), an *estimate* of the magnitude of the advective heat transfer due to a flow field with a volume rate of flow proportional to $\delta \cdot U_\sigma$, circulating between regions that have a temperature difference of ΔT can be calculated. Because advective effects are modeled here using a conduction code, the advective heat transfer is cast as conduction heat transfer due to an average temperature gradient given by $\Delta T/L$ where L is the weld pool width. The resulting equation for effective thermal conductivity, including both advec-

tive and conductive effects, is given by Eqn. (5). It has been shown that values of k given by Eqn. (5) are of the same order of magnitude as empirically determined values reported in the literature (Kanouff, 1994). It is re-emphasized that this method for modeling thermal energy transport within the weld pool is approximate. However, because pool thermal response is not of interest here, it is deemed adequate. In all simulations, Eqn (5) was evaluated with L = 1.0 mm (measured weld pool widths ranged from 0.6 to 1.0 mm for the parameters considered here).

The computations incorporate linear finite elements and are performed on 57,000 and 78,000 node meshes for the development and process model simulations respectively. The mesh is designed so that dense mesh packing is included in the weld travel path to resolve the expected high temperature gradients within this region. Halving the number of nodes in both development and process model simulations results in less than a two percent change in $T_{d,1}$ and $T_{p,1}$ (see Figs. 1 and 2) dimensionless temperature, θ.

RESULTS AND DISCUSSION

Experimental measurements and numerical predictions are presented below. Model development results are presented first, followed by the actual process measured and simulated results.

Model Development Measurements and Simulations

Results are obtained for the range parameters given in Table 4. Measured thermal response histories are shown in Fig. 3 (data points are shown at $\Delta t = 3.0 \times 10^{-3}$ s). Figure 3 (a) shows the "near-field" thermal response history, $T_{d,1}$, at x = 7.8 mm, directly underneath the weld bead while Fig. 3 (b) displays the "far-field" response history, $T_{d,2}$, at a location x = 7.8 mm, y = 3 mm (see Fig. 1). Temperatures were also measured at locations x = 2.8 and 12.8 mm (same y's) and found to be the same as $T_{d,1}$ and $T_{d,2}$ (translated in time) within the experimental repeatability,

and so are not reported here. Note that the results of Fig. 3 are translated in time such that the peak $T_{d,1}$ occurs at t = 0 s (in order to eliminate uncertainty in laser start times).

As the laser begins translating across the part, the measured $T_{d,1}$ (Fig. 3 (a)) initially shows negligible change as thermal energy diffuses forward much slower than it is advected due to translation of the laser beam ($Pe = 2 \times 10^6 >> 1$). As the beam passes over $T_{d,1}$, its temperature increases dramatically, with $T_{d,1}$ increasing with increasing P_{peak} at any time, t. This dependence of part temperature on P_{peak} results because only a fraction of the beam energy is absorbed by the part. The ratio of absorbed energy to beam energy is the energy transfer efficiency of the process,

$$ETE = \frac{P_{a,avg}}{P_{avg}} \tag{8}$$

where $P_{a,avg}$ is the absorbed (average) beam energy and P_{avg} is the actual average beam energy. Energy transfer efficiency is unique for a given set of processing conditions, depending on parameters including weld pool and metal vapor radiative properties, laser wavelength, weld pool geometry and extent of the metal vapor plume (Fuerschbach, 1996; Fuerschbach and MacCallum, 1995). Generally, weld pool geometry and metal vapor extent are related to peak laser pulse power since P_{peak} determines rate of melt circulation and metal vaporization which, in turn, modify weld pool surface depression (Oreper and Szekely, 1984; Semak et al, 1994). For these reasons, workpiece temperature is a function of P_{peak}.

After the laser passes over the $T_{d,1}$ location, Fig. 3 (a) shows that $T_{d,1}$ decreases rapidly as energy is conducted away to cooler regions of the part (and lost to the environment). As in the earlier stages of the process, cases corresponding to higher P_{peak} show an increased $T_{d,1}$ at any time.

Figure 3 (b) illustrates the far-field thermal response; $T_{d,2}$, of the part and shows a signifi-

cant decrease in peak temperature relative to the $T_{d,1}$ response at all P_{peak} values. However, as with the $T_{d,1}$ thermal response, the $T_{d,2}$ history indicates a *generally* increasing temperature with increased P_{peak} values (at any t). Again, this is thought to be a result of increased ETE.

Because of the complex coupled mechanics involved, determination of ETE from first principles is practically impossible. For this reason, the experimental results of Fig. 3 along with simulations are used to estimate the ETE at each experimental P_{peak}. Specifically, the development model is run at each P_{peak} value and ETE values are adjusted until the $T_{d,1}$ and $T_{d,2}$ histories are matched within the experimental uncertainties.

Development model predictions are shown in Figure 4. Because ETE was adjusted to match experimental (Fig. 3) and predicted (Fig. 4) results, it is not surprising that comparison is relatively good over most of the history. Unfortunately, it was found that peak $T_{d,1}$ temperatures could not be predicted while matching the remaining portions of the thermal histories. It is speculated that this error is due, in part, to the large thermal mass of the thermocouple bead (diameter $\approx$ 600 μm) relative to that of the weld pool (d $\approx$ 900 μm).

The ETE and P_{peak} relation derived from the development measurements and predictions is shown in Fig. 5. Note that at low values of P_{peak} (< 1680 W) ETE is constant at 0.36. This behavior may be a result of low vapor production at the lower power level, resulting in minimal vapor-beam interaction and weld pool depression. Thus, for relatively low values of P_{peak}, beam absorption is mainly a function of melt absorptivity. Of course, care should be exercised when using these values of ETE since they where obtained for a specific process over a specific range of P_{peak}.

Process Measurements and Simulations

A set of simulations have been performed to examine the accuracy of the heat input model when applied to an actual component being pulsed Nd:YAG laser welded. The process parameters considered are given in Table 5. The predicted thermal responses are compared to measured data to assess the accuracy of the model.

Measured and predicted thermal response histories for the $P_{peak} = 1390$ W case are shown in Fig. 6 (data points are shown at $\Delta t = 5.0 \times 10^{-3}$ s). Measured and predicted (solid and dashed-lines respectively) temperature histories are provided for the header ($T_{p,1}$ and $T_{p,2}$), ferrule ($T_{p,3}$) and case ($T_{p,4}$) locations (see Fig. 2). Figure 6 shows that the predictions match the measured response reasonably well. However, case and header temperature histories are all underpredicted (except at early time) while the ferrule temperature is overpredicted. The discrepancy in case temperature may be the result of the laser beam shining over the edge of the part, resulting in a larger portion of the beam's energy being deposited in the case. It should be noted that maintaining precise (fraction of a millimeter) alignment of the laser beam and workpiece during translation is extremely difficult. This loss of laser alignment can be seen as a spike in the thermal history of $T_{p,4}$ as the beam passes ($t = 1$ s). It is not clear at this time why the model overpredicts the response at $T_{p,3}$. The lack of a detailed interfacial model (perfect contact is assumed) near the ferrule-glass-pin location may be partially responsible for the differences.

Figure 7 shows thermal response histories for $P_{peak} = 830$ W at locations corresponding to those of Fig. 6. A comparison of Fig. 6 and Fig. 7 reveals a negligible change in thermal response histories for the corresponding change in P_{peak} as ETE remains unchanged (see Fig. 5). Fig. 7 again demonstrates the ability of the model to qualitatively predict the thermal response of the component during pulsed laser welding. Again, the model tends to underpredict the measured

case and header response while overpredicting ferrule thermal response. The reasons for the differences between predicted and measured temperatures cited for the P_{peak} = 1390 W case are applicable to this case as well.

CONCLUSIONS

An experimental and numerical study is conducted to analyze the thermal response of a part subject to pulsed Nd:YAG laser welding. Experiments performed for a simple system, along with concurrent development model predictions, illustrate the relationship between energy transfer efficiency and laser peak pulse power. The results indicate that, for the parameters and system considered, energy transfer efficiency is effectively constant for relatively low peak powers and then increases once a threshold power is reached. The constant energy transfer efficiency region may be attributable to surface absorption and reflection of the laser energy. Once the threshold value is reached, transfer efficiency increases as the weld pool surface depresses, increasing exposed surface area and hence increasing beam absorption. These trends are consistent with results obtained for continuous wave welding processes reported in the literature.

A numerical process model is developed, using the energy transfer efficiency-peak power relation generated from the development experiments. The process model is capable of estimating the thermal response of an actual electronic component during the welding process. Experiments and simulations are performed for two peak power levels and the measurements and predictions compared favorably.

The model developed here is intended to provide rapid thermal history results to welding engineers to help guide them in welding hermetic containers to reduce thermal and (when coupled with a mechanical model) mechanical damage to the part of interest. Although this should be very

useful, further advancements in the model are warranted. For example, although weld pool geometry is important to the welding engineer (e.g. how deep is the weld?), no such information is provided by this model. Again, accurate prediction of weld pool physics, and hence weld pool shape, require detailed understanding of the complex physics involved. It is not clear at this time how these effects can (or if they can) be modeled with the simple approach adopted here. More work in this area is needed to address these issues.

ACKNOWLEDGEMENTS

The authors would like to thank C. Frysz, A. Honegger and J. Spaulding for their invaluable input throughout this work and J. Gajewski for providing metallurgical support. This work was supported in part by the United States Department of Energy under contract DE-AC04-94ALB500.

REFERENCES

Chen, M.M., 1987, "Thermocapillary Convection in Materials Processing," in *Interdisciplinary Issues in Materials Processing and Manufacturing*, S.K. Samanta et al. eds., Vol. 2, pp. 541-558.

Choi, M. Greif, R. and Salcudean, M., 1987, "A Study of the Heat Transfer During Arc Welding with Applications to Pure Metals or Alloys and Low or High Boiling Temperatures," *Numerical Heat Transfer*, Vol. 11, pp. 477-489.

Fuerschbach, P.W. and MacCallum, D.O., 1995, "Variation of Laser Energy Transfer Efficiency with Weld Pool Depth," ICALEO LIA: San Diego, CA.

Fuerschbach, P.W., 1996, "Measurement and Prediction of Energy Transfer Efficiency in Laser Beam Welding," *Welding Journal*, Vol. 75(1), pp. 24s-34s

Fuerschbach, P.W. and Hinkley, D. A. 1997, "Pulsed Nd:YAG Laser Welding of Heart Pacemaker Batteries with Reduced Heat Input," *Welding Journal* (Accepted for publication).

Gartling, D.K. and Hogan, R.E., 1994, *COYOTE - A Finite Element Computer Program for Nonlinear Heat Conduction Problems, Sandia Report SAND94-1173*, Sandia National Laboratories, NM.

Gianoulakis, S.E., Burchett, S.N., Fuerschbach, P.W. and Knorovsky, G.A., 1995, "The Effect of Travel Speed on Thermal Response in CO_2 Laser Welding of Small Electronic Components," in *Proceedings of the 1995 ASME National Heat Transfer Conference*, Vol. 4, pp. 249 - 254.

Honegger, A. E., 1996, Personal Communication, Wilson Greatbatch Ltd.

Incropera, F.P. and DeWitt, D.P., 1990, *Fundamentals of Heat and Mass Transfer*, 3rd ed., John Wiley & Sons, New York.

Kanouff, M.P. and Greif, R., 1992, "The Unsteady Development of a GTA Weld Pool," *International Journal of Heat and Mass Transfer*, Vol. 35, pp. 967-979.

Kanouff, M.P., 1994, "The Effective Thermal Conductivity in Weld Pools," Sandia Memorandum, April 27, Sandia National Laboratories, NM.

Knorovsky, G. A. and Burchett, S. N., 1989, "The Effect of Heat Sinks in GTA Microwelding," *Proceedings of the 2nd International Conference on Trends in Welding Research*, pp 469-474.

Oreper, G.M. and Szekely, J., 1984, "Heat- and Fluid-Flow Phenomena in Weld Pools," *Journal of Fluid Mechanics*, Vol. 147, pp. 53-79.

Ostrach, S., 1982, "Low-Gravity Fluid Flows," *Annual Review of Fluid Mechanics*, Vol. 14, pp. 313-345.

Root, R.G., 1980, "Laser Interaction: Thermal and Mechanical Coupling to Targets," *Journal de Physique*, Vol. 41, pp. c59-c73.

Russo, A.J., Akau, R.L. and Jellison, J.L., 1990, "Thermocapillary Flow in Pulsed Laser Beam Weld Pools," *Welding Research Supplement*, pp. 23s-29s.

Semak, V.V., Hopkins, J.A., McCay, M.H. and McCay, T.D., 1994, "A Concept for a Hydrodynamic Model of Keyhole Formation and Support During Laser Welding," in *Proceedings of the Laser Materials Processing Conference, ICALEO '94*, Vol. 79, T.D. McCay et al. eds., LIA, Orlando, FL.

Seraphim, D.P., Lasky, R. and Li, C-Y., 1989, *Principles of Electronic Packaging*, McGraw-Hill, New York.

Siegel, R. and Howell, J.R., 1992, *Thermal Radiation Heat Transfer*, 3rd ed., Hemisphere Publishing, Washington.

Weast, R.C., 1966, *Handbook of Chemistry and Physics*, 47th ed., CRC Press, Boca Raton, FL.

Zienkiewicz, O.C. and Taylor, R.L., 1991, *The Finite Element Method, Vol. 2,* 4th ed., McGraw-Hill, London.

FIGURE TITLES

Figure 1 - Schematic of development apparatus and computational domain.

Figure 2 - Schematic of process apparatus and computational domain.

Figure 3 - Development experiment measured thermal response histories at locations x = 10 mm (a) directly under the weld path (y = 0 mm; $T_{d,1}$) and (b) at an offset from the weld path (y = 3mm; $T_{d,2}$).

Figure 4 - Development experiment predicted thermal response histories at locations x = 10 mm (a) directly under the weld path (y = 0 mm) and (b) at an offset from the weld path (y = 3mm).

Figure 5 - Energy transfer efficiency (ETE) as a function of peak laser power for use in predictions.

Figure 6 - Process experiment predicted and measured component thermal response histories for the lid ($T_{p,1}$ and $T_{p,2}$), ferrule ($T_{p,3}$) and case ($T_{p,4}$) locations shown in Figure 2 with P_{peak} = 1390 W (f = 83 Hz). Dashed line = predictions, solid line = measurements

Figure 7 - Process experiment predicted and measured component thermal response histories for the header ($T_{p,1}$ and $T_{p,2}$), ferrule ($T_{p,3}$) and case ($T_{p,4}$) locations shown in Figure 2 with P_{peak} = 830 W (f = 138 Hz). Dashed line = predictions, solid line = measurements

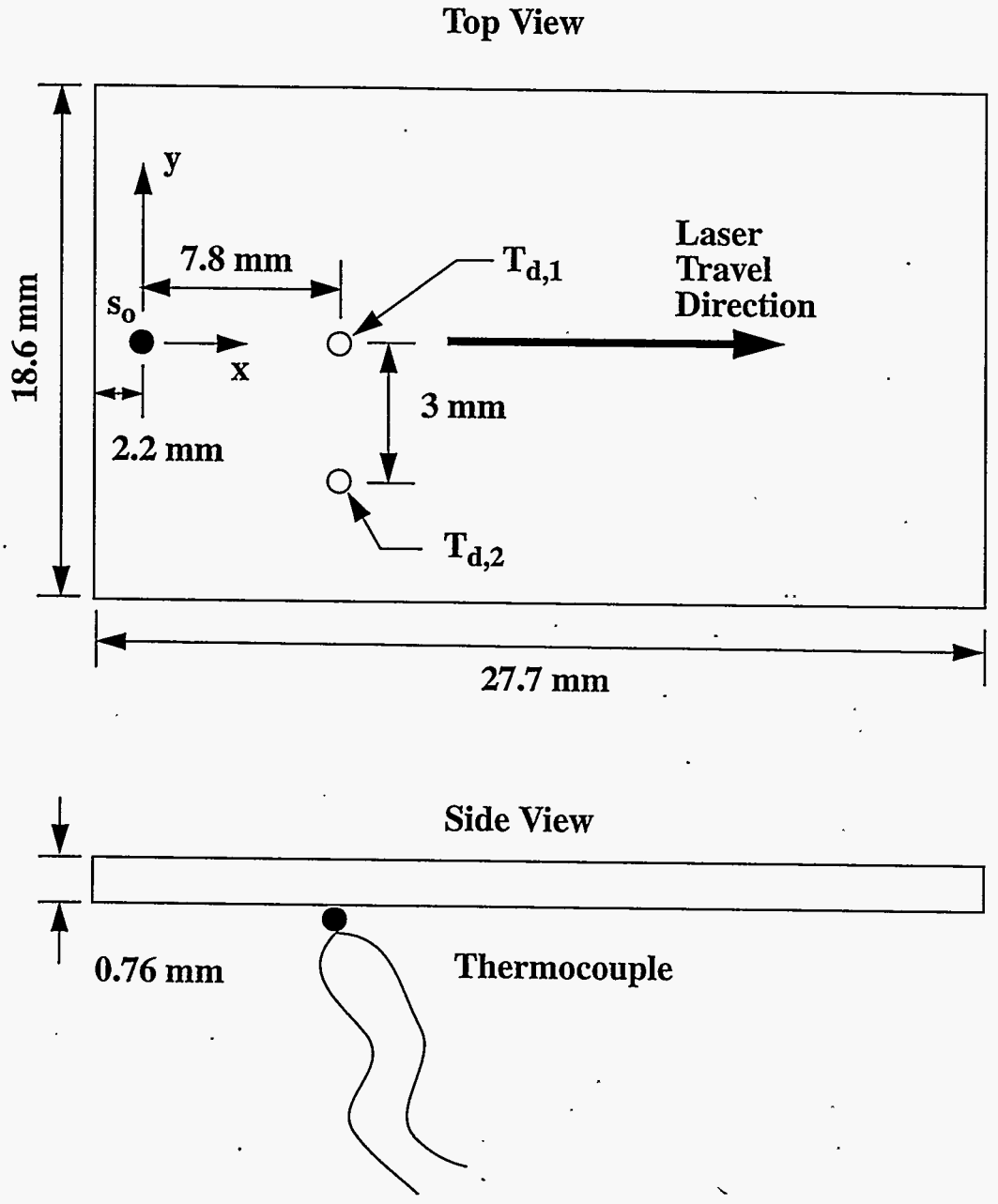

Figure 1 - Gianoulakis et al.

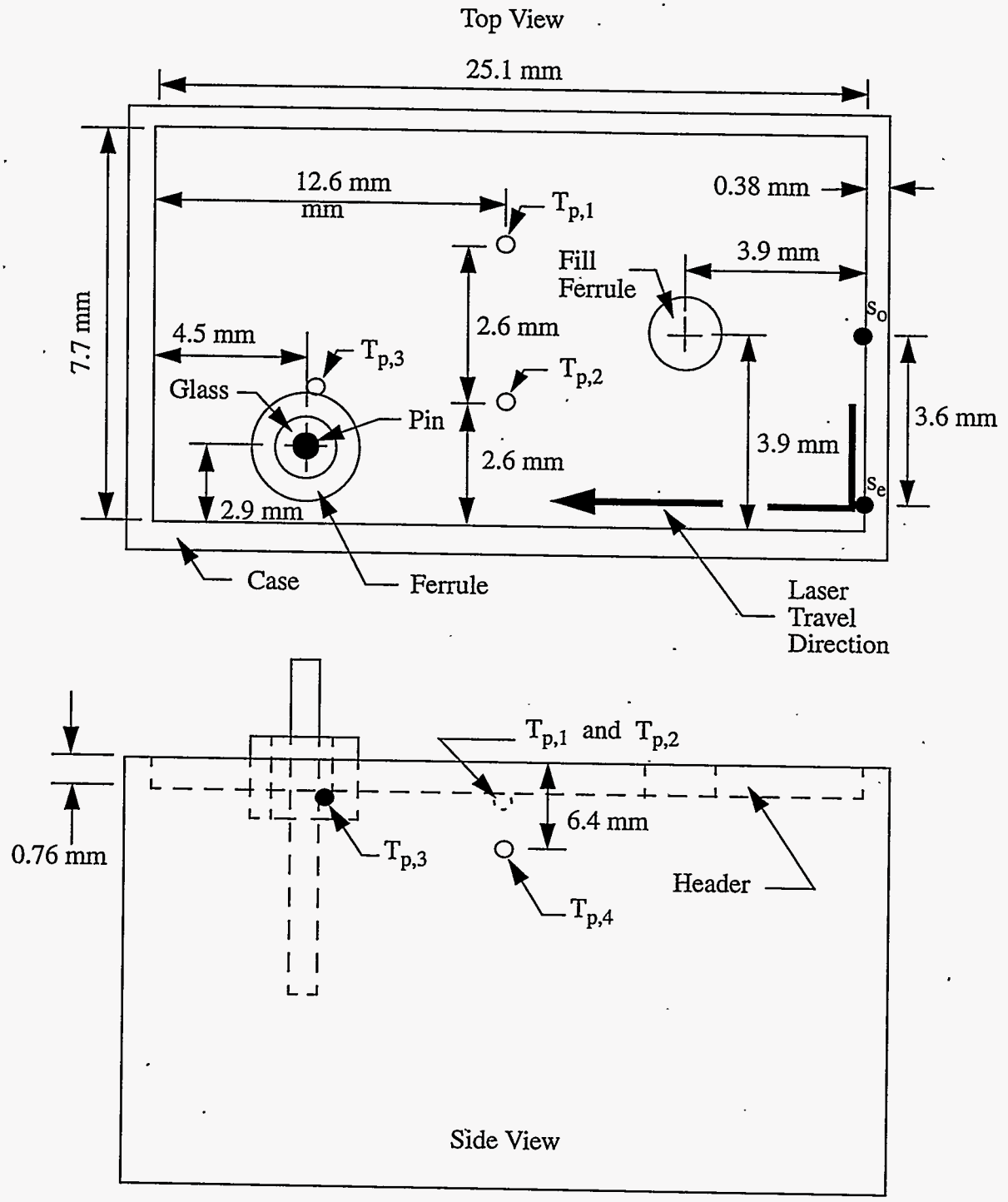

Figure 2 - Gianoulakis et al.

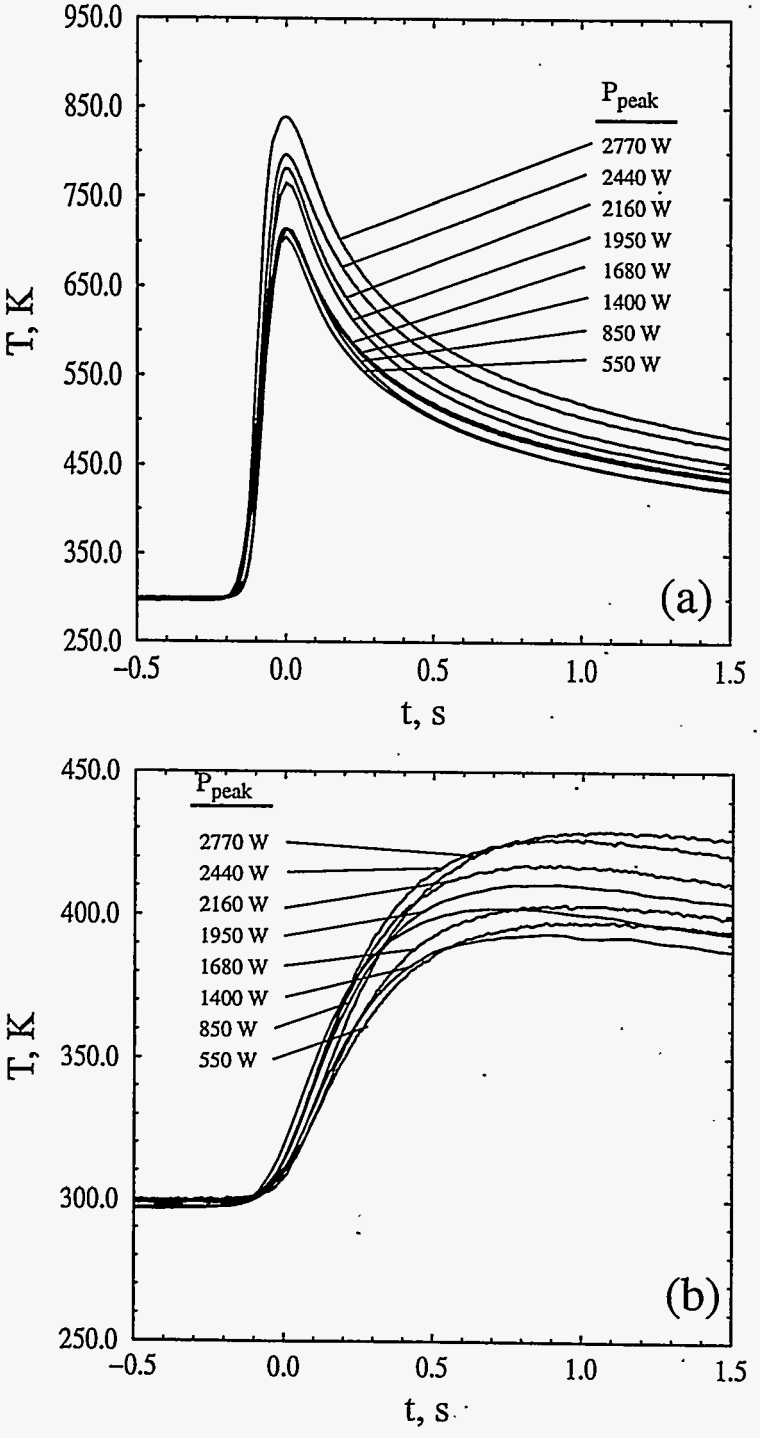

Figure 3 - Gianoulakis et al.

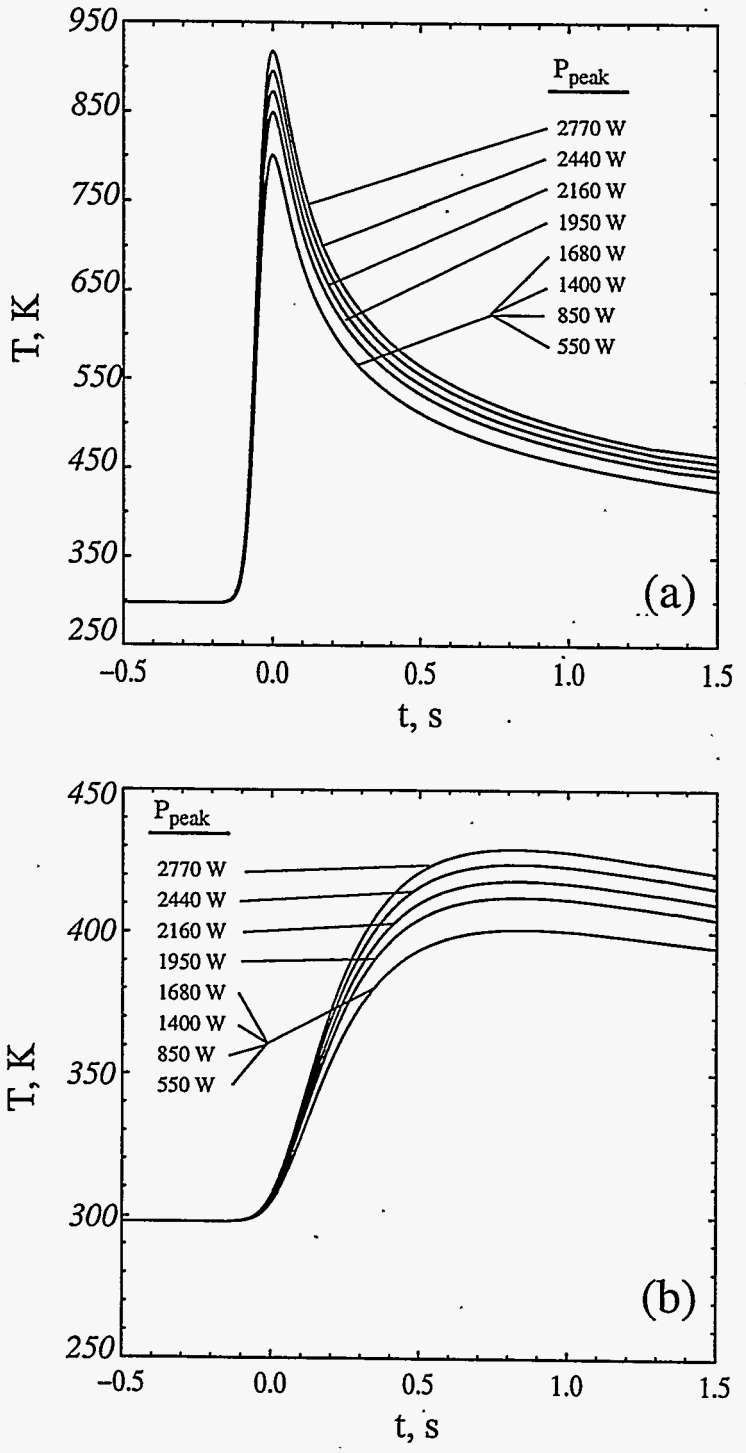

Figure 4 - Gianoulakis et al.

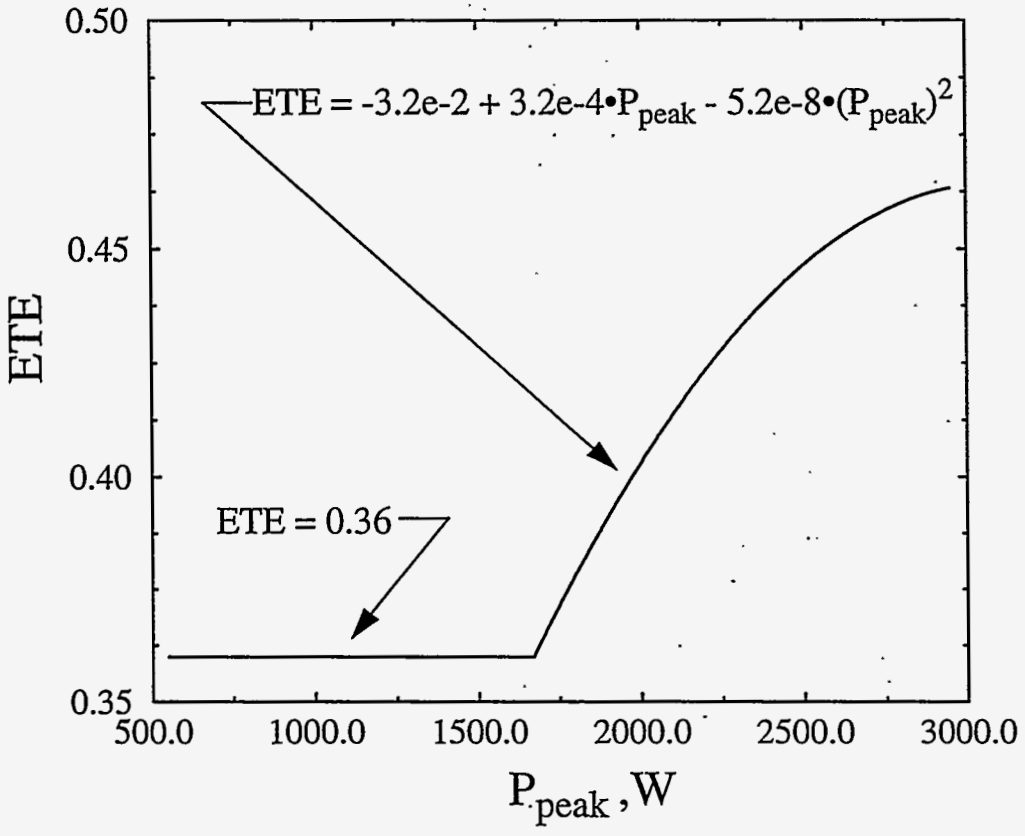

Figure 5 - Gianoulakis et al.

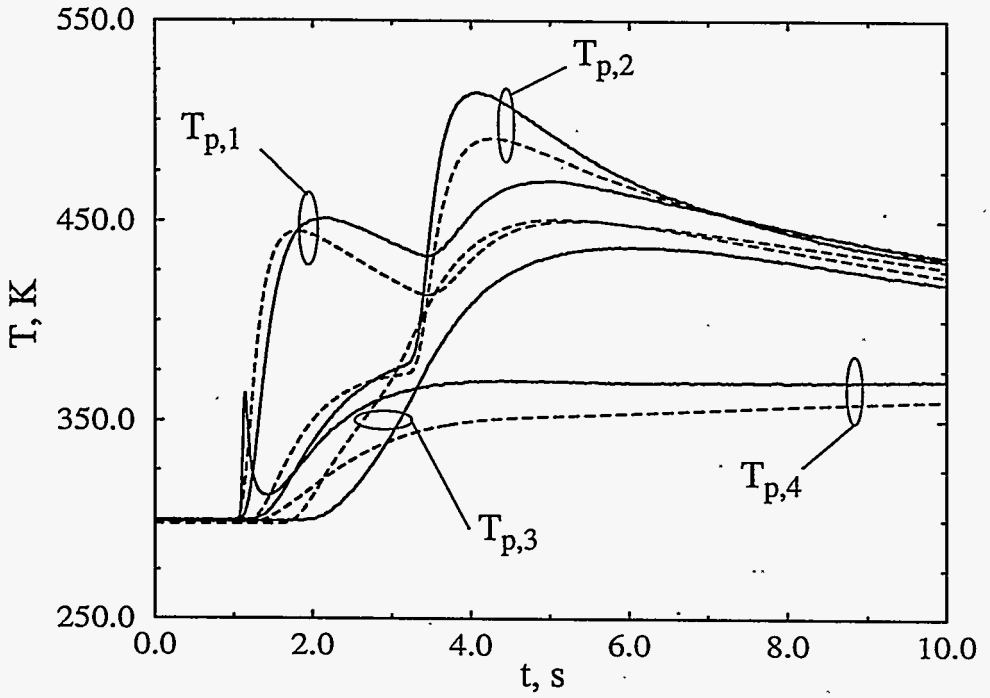

Figure 6 - Gianoulakis et al.

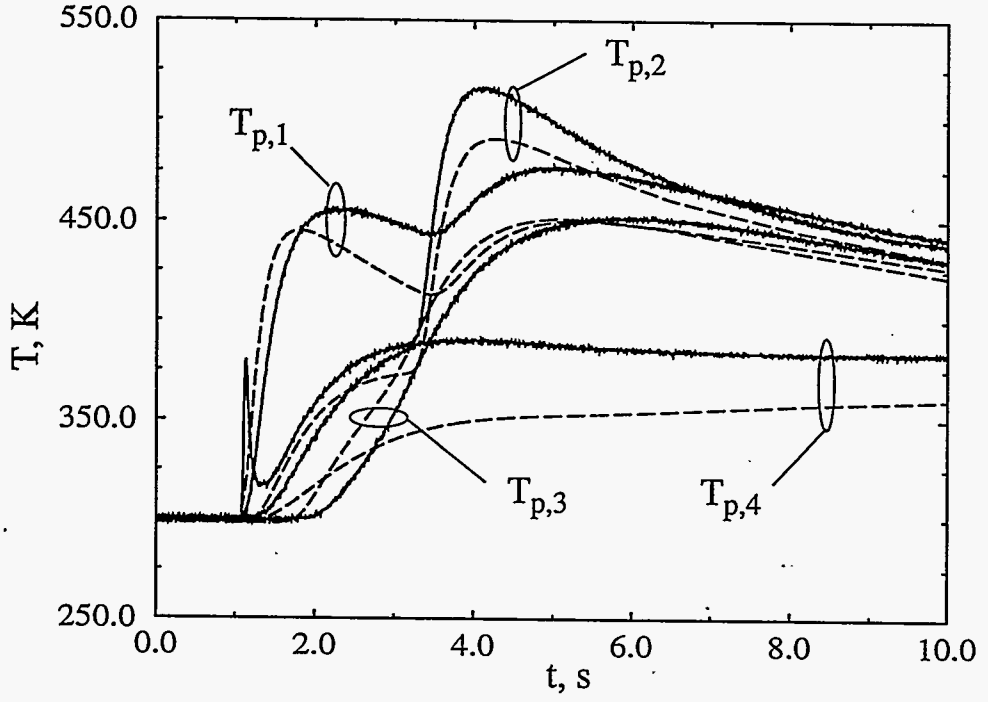

Figure 7 - Gianoulakis et al.

Table 1: 304 Stainless Steel Thermal Properties*

T (K)	ρ (kg/m^3)	c (J/kg•K)	k (W/m•K)
0	7820	465	8.12
1670	7820	689	27.0
1730	6862	788	17.9
2500	6862	788	28.5
* Choi et al., 1987			

Table 2: Glass Thermal Properties*

T (K)	ρ (kg/m^3)	c (J/kg•K)	k (W/m•K)
0	2300	710	1.26
373	---	858	1.26
773	---	1109	1.88
1073	---	1214	1.88
1973	---	1465	2.60
2500	2300	1465	2.60
* Weast, 1966			

Table 3: Molybdenum Thermal Properties*

T (K)	ρ (kg/m^3)	c (J/kg•K)	k (W/m•K)
100	10240	141	17.9
400	---	261	13.4
800	---	285	11.8
1200	---	308	10.5
2500	10240	459	8.6
* Incropera and DeWitt, 1990			

Table 4: Model Development Experiment Parameters

P_{peak} (W)	f (pulse/s)	E (J/pulse)
550	208	0.715
830	138	1.08
1390	83.0	1.81
1680	69.2	2.18
1950	59.3	2.54
2160	51.9	2.81
2440	46.1	3.17
2770	41.5	3.60
d = 15.2 mm/s, f = 160 mm, P_{avg} = 150 W, $t_{pd} = 1.3 \times 10^{-3}$ s, V = 15.2 mm/s		

Table 5: Process Experiment Parameters

P_{peak} (W)	f (pulse/s)	E (J/pulse)
830	138	1.08
1390	83.0	1.81
d = 15.2 mm/s, f = 160 mm, P_{avg} = 150 W, $t_{pd} = 1.3 \times 10^{-3}$ s, V = 15.2 mm/s		